A NUMERICAL ALGORITHM FOR ENDOCHRONIC PLASTICITY AND COMPARISON WITH EXPERIMENT

K.C. Valanis and Jinghong Fan
University of Cincinnati
Cincinnati, Ohio 45221

A numerical algorithm based on the finite element method of analysis of the boundary value problem in a continuum is presented, in the case where the plastic response of the material is given in the context of endochronic plasticity. The relevant constitutive equation is expressed in incremental form and plastic effects are accounted for by the method of an induced pseudo-force in the matrix equations.

The results of the analysis are compared with observed values in the case of a plate with two symmetric notches and loaded longitudinally in its own plane. The agreement between theory and experiment is excellent.

INTRODUCTION

The greatest difficulty encountered in the application of the classical theory of plasticity is the lack of knowledge of the configuration of the subsequent yield surface for the particular material at hand, and the experimental difficulties encountered in finding it in the fully three dimensional case. More importantly, however,

it has been observed by many experimenters that the shape of the subsequent yield surface and its position in stress space depends very strongly on the definition of the yield point, particularly in situations following prior deformation [1-3].

The essential premise of the classical plasticity theory is the assumption of an a priori existence of a yield surface. This implies a finite elastic domain. From the mathematical standpoint, a finite domain is necessary because of the requirement that the increment in plastic strain be normal to the yield surface. Thus, the direction of the plastic strain increment is dictated by the yield surface configuration.

If plastic effects were to begin immediately upon loading, perforce, the domain of the yield surface would collapse to a point, thus making the direction of the plastic strain increment indeterminate since all directions are normal to a point. Thus, the classical plasticity theory cannot deal with materials that yield immediately upon loading. There are other difficulties associated with experimental attempts to describe and analyze a two-or three-dimensional response of a material [4]. For instance, investigations in the hardening rule are much discussed in the current literature, but definitive functional forms outside the Prager-Ziegler rule are very few, and lack firm experimental verification. This rule specifically can have only limited application, and is inappropriate for

complicated loading histories. Moreover, it gives rise to large discrepancies between calculated and experimental data in loading-unloading processes [1]. Other numerical difficulties arise from the fact that the loading increments cannot be assigned arbitrarily a priori. When the current loading increment makes the stress state of a particular element traverse the yield surface it is necessary to come back to the preyious loading state and adjust the magnitude of the new increment of loading to ensure that the new stress state is located just on the yield surface. Certainly, this process increases the time of computation.

In 1971, Valanis proposed an alternative theory of viscoplasticity called "endochronic theory" [5,6], which is based on irreversible thermodynamics and the concept of intrinsic time. The theory provides a unified point of view to describe the elastic-plastic behavior of materials since it places no requirement for a yield surface and a "loading function" to distinguish between loading and unloading.

In a series of recent works, Valanis, Wu and others [7-10] demonstrated that the endochronic theory could apply more precisely to situations involving unloading and cyclic behavior of metals, as well as wave propagation in the plastic region.

However, in all of the works, involving more than one dimension, where the loading was quasi-static, the stress fields were homogeneous.

In the present paper a numerical algorithm is first implemented in a computer program, which can be used to analyze the material response in monotonic and cyclic loading in the case of plane stress or plane strain. The calculated results are then compared with the data obtained from a specially designed experiment on a notched plate cyclically loaded in its own plane. The validity of the endochronic analysis, using this numerical algorithm, is thereby demonstrated.

AN INCREMENTAL FORM OF THE ENDOCHRONIC ELASTOPLASTIC CONSTITUTIVE EQUATION IN TERMS OF {dσ} and {dε}

The following are the formulae concerning the endochronic constitutive equations for plastically incompressible isotropic materials and small deformation [7]

$$\underset{\sim}{s} = \int_0^z \rho(z-z') \frac{\partial \underset{\sim}{e}^p}{dz'} dz' \tag{2.1}$$

$$d\zeta = \|de^p\| \tag{2.1a}$$

$$dz = \frac{d\zeta}{f(\zeta)} \tag{2.1b}$$

where $\rho(z)$ and $f(\zeta)$ are two material functions namely the kernel function and hardening function respectively.

$$\sigma_{kk} = 3K\varepsilon_{kk} \tag{2.2}$$

$$\underset{\sim}{de}^{p} = \underset{\sim}{de} - \frac{1}{2\mu}\,\underset{\sim}{ds} \tag{2.3}$$

By definition

$$de_{ij} = d\varepsilon_{ij} - \frac{1}{3}\,d\varepsilon_{\alpha\alpha}\delta_{ij} \tag{2.4a}$$

$$ds_{ij} = d\sigma_{ij} - \frac{1}{3}\,d\sigma_{\alpha\alpha}\delta_{ij} \tag{2.4b}$$

In this paper the form of $\rho(z)$ given by equation (2.5) was used in equation (2.1)

$$\rho(z) = \sum_{r=1}^{\infty} c_r e^{-\alpha_r z} \tag{2.5}$$

with the conditions that β_r and R_r are positive for all r and

$$\sum_{r=1}^{\infty} c_r = \infty\,, \qquad \sum_{r=1}^{\infty} \frac{c_r}{\alpha_r} < \infty\,. \tag{2.6a,b}$$

This form of $\rho(z)$ is continuous and differentiable in $(0,\infty)$ and therefore the incremental form of equation (2.1) specified below can be used in conjunction with a finite element code.

Specifically in the case where the infinitely large value of $\rho(0)$ is approximated by a suitably large value, as is done in this paper, one may differentiate equation (2.1) with respect to z to obtain the following differential form of the endochronic constitutive equation:

$$\underset{\sim}{ds} = \rho(0)\,\underset{\sim}{de}^{p} + \underset{\sim}{h}(z)\,dz \tag{2.7}$$

where

$$\underset{\sim}{h}(z) = \int_{0}^{z} \hat{\rho}(z-z')\,\frac{\partial \underset{\sim}{e}^{p}}{\partial z'}\,dz' \tag{2.8}$$

and

$$\hat{\rho}(z) = \frac{d\rho}{dz} \tag{2.8a}$$

The elastoplastic constitutive equations (2.3) and (2.7), can then be combined and expressed in the differential form

$$ds_{ij} = 2\hat{\mu}\{de_{ij} + \frac{1}{\rho(0)} h_{ij}(z)dz\} \tag{2.9}$$

where

$$\hat{\mu} = \rho(0) \{1 + \frac{\rho(0)}{2\mu}\}^{-1} \tag{2.9a}$$

Alternately, for computational purposes the incremental form given by equation (2.10) may be used, i.e.,

$$\Delta s_{ij} = 2\hat{\mu} \{\Delta e_{ij} + \frac{1}{\rho(0)} h_{ij}(z) \Delta z\} \tag{2.10}$$

Substituting (2.4a,b) into (2.9) and using (2.2) one obtains the operational incremental form of the elastoplastic constitutive equation in matrix notation as follows:

$$\{d\sigma\} = \{D\} \{d\varepsilon\} + \{dH_p\} \tag{2.11}$$

where

$$\{D\} = \begin{bmatrix} c_1 & c_2 & 0 \\ c_2 & c_1 & 0 \\ 0 & 0 & \hat{\mu}_p \end{bmatrix} \tag{2.12}$$

and

$$\{dH_p\} = \begin{Bmatrix} dH_{px} \\ dH_{py} \\ dH_{pxy} \end{Bmatrix} \tag{2.13}$$

In plane stress

$$c_1 = \frac{12K\hat{\mu} + 4\hat{\mu}^2}{3K + 4\mu} \tag{2.14}$$

$$c_2 = \frac{6K\hat{\mu} - 4\hat{\mu}^2}{3K + 4\mu} \tag{2.15}$$

$$D_1 = \frac{2\hat{\mu}(3k-2\hat{\mu})}{3k + 4\mu} \tag{2.16}$$

$$dH_{px} = \{2\hat{\mu}h_x(z) - D_1h_z(z)\}\, dz/\rho(0) \tag{2.17}$$

$$dH_{py} = \{2\hat{\mu}h_y(z) - D_1h_z(z)\}\, dz/\rho(0) \tag{2.18}$$

$$dH_{pxy} = 2\hat{\mu}h_{xy}(z)dz/\rho(0) \tag{2.19}$$

In plane strain

$$c_1 = \frac{3K + 4\hat{\mu}}{3} \tag{2.20}$$

$$c_2 = \frac{3K - 2\hat{\mu}}{3} \tag{2.21}$$

$$dH_{px} = 2\hat{\mu}\, h_x(z)\,dz/\rho(0) \tag{2.22}$$

$$dH_{py} = 2\hat{\mu}\, h_y(z)\,dz/\rho(0) \tag{2.23}$$

$$dH_{xy} = 2\hat{\mu}\, h_{xy}(z)\,dz/\rho(0) \tag{2.24}$$

We note that {D} is an adequate approximation to the elastic matrix {E}. It is evident from equation (2.9a) that when $\rho(0) \to \infty$, {D} becomes the elastic matrix {E}. Take plane stress as an example on the simple tension curve (Fig. 1) draw

$$\lim_{\rho(0)\to\infty} \{D\} = \{E\} = \frac{E}{2(1+\nu)(1-\nu)} \begin{Bmatrix} 2 & 2\nu & 0 \\ 2\nu & 2 & 0 \\ 0 & 0 & (1-\nu) \end{Bmatrix} \tag{2.25}$$

We use axial tension to show the geometric meaning of equation (2.11). From a point A on simple tension curve (Fig. 1) draw a straight line AB, the slope of which is Young's modulus E and its horizontal projection is $d\varepsilon$. For simple tension

$$\{D\}\{d\varepsilon\} = E d\varepsilon \tag{2.26}$$

and

$$BD = E d\varepsilon$$

so BD can be considered as the first term of right hand in (2.11). Since CD is equal to $d\sigma$, the geometric meaning of dH_p is represented by the segment BC the value of which is negative for simple tension.

Using (2.11) and the principle of virtual work [11], one may formulate an initial stress finite element computational algorithm of the endochronic theory. In fact, we have

$$\iiint_V \{\sigma\}^T \{\delta\varepsilon\} dv = \{p_{ex}\}^T \delta\{q\} \tag{3.1}$$

and $\{p_{ex}\}$ and $\{q\}$ are respectively the vectors of nodal external forces and displacements of the element. Substituting (2.11) into (3.1) one finds that

$$\{K\}\ \{\Delta q\} = \{\Delta p_{ex}\} + \{\Delta p_p\} \tag{3.2}$$

where $\{K\}$ is the stiffness matrix of the element and is the same as the stiffness matrix of an element in the usual elastic analysis but the constants C_1, C_2 are obtained from equations (2.14 - 2.16) or (2.20 - 2.21).

The quantity $\{\Delta P_p\}$ is the incremental plastic pseudo-force vector for a typical triangular element used in the analysis and has the form

$$\begin{aligned} (\Delta P_{px})_i &= -\frac{t}{2}\,(\alpha_i \Delta H_{px} + \beta_i \Delta H_{pxy}) \\ & \qquad\qquad\qquad\qquad i = 1,2,3 \qquad (3.3) \\ (\Delta P_{py})_i &= -\frac{t}{2}\,(\beta_i \Delta H_{py} + \alpha_i \Delta H_{pxy}) \end{aligned}$$

Where the components of $\{\Delta H_p\}$ are given in equations (2.17 -19) or (2.22-24) by changing operator "d" to "Δ". α_i and β_i are related to the differences of nodal coordinates, i.e.,

$$\alpha_i = \frac{1}{2} e_{ijk}\Delta y_{jk} \quad , \quad \beta_i = -\frac{1}{2} e_{ijk}\Delta x_{jk} \qquad (i = 1,2,3) \tag{3.4}$$

where $\Delta y_{jk} = y_j - y_k$, $\Delta x_{jk} = x_j - x_k$ and e_{ijk} is the permutation symbol.

From equations (3.2) and (3.3) one obtains the total stiffness matrix $\{k\}$, total plastic pseudo force matrix $\sum\{\Delta P_p\}$ and the linear simultaneous equations for the structure.

THE CALCULATION OF h(z)

Equations (2.17) through (2.19) show that $\underset{\sim}{h}(z)$ plays a central role in the calculation of $\{\Delta H_p\}$ and plastic pseudo-force $\{\Delta P_p\}$. To calculate h(z) numerically, we divide the domain of integration (0,z) in equation (2.8) into n subregions whereupon

$$h(z_m) = \int_0^{z_1} \hat{\rho}(z_m - z') \frac{\partial \underset{\sim}{e}^p}{\partial z'} dz' \ldots\ldots + \int_{z_{i-1}}^{z_i} \hat{\rho}(z_m - z') \frac{\partial \underset{\sim}{e}^p}{\partial z'} dz' \ldots\ldots$$

$$\ldots + \int_{z_{m-1}}^{z_m} \hat{\rho}(z_m - z') \frac{\partial \underset{\sim}{e}^p}{\partial z'} dz' \tag{4.1}$$

where z_{i-1}, z_i are the intial and end values, respectively, of the intrinsic time scale of ith interval, which corresponds

to the ith incremental loading process, and z_m is the current value of the intrinsic time scale.

The mean value theorem, and the smoothness of $\underset{\sim}{e}^p$ allows the approximation

$$\int_{z_{i-1}}^{z_i} \hat{\rho}(z_m - z')\, \frac{\partial \underset{\sim}{e}^p}{\partial z'}\, dz' \approx \left.\frac{\partial \underset{\sim}{e}^p}{\partial z}\right|_{z=z_i} \int_{z_{i-1}}^{z_i} \hat{\rho}(z_m - z')\, dz' \tag{4.2}$$

provided that there is no strain reversal in the interval considered. In the present work we approximate the series on the right hand side of equation (2.5) by three terms, i.e.,

$$\rho(z) = \sum_{r=1}^{3} C_r e^{-\alpha_r z} \tag{4.3}$$

Substituting equation (4.3) into equation (4.1) and using equation (4.2) we obtain the result

$$\underset{\sim}{h}(z_m) = \sum_{r=1}^{3} \sum_{i=1}^{m} C_r \left.\frac{\partial \underset{\sim}{e}^p}{\partial z}\right|_{z=z_i} e^{-\alpha_r (z_m - z_{i-1})} \left[1 - e^{\alpha_r (z_i - z_{i-1})}\right] \tag{4.4}$$

This form of $\underset{\sim}{h}$ is unsuitable for numerical compulation. The term $\alpha_r(z_m - z_{i-1})$ may in the course of calculation become very large of ther order of 5×10^4. Consequently, the value of the function $\exp\{-\alpha_r(z_m - z_{i-1})\}$ becomes a very small number leading to serious truncation errors. To avoid this difficulty we proceed as follows. By mathematical induction the following formula can be shown:

$$\underset{\sim}{h}(z_i) = \sum_{r=1}^{3} \underset{\sim}{h}(z_{i-1})e^{-\alpha_r \Delta z_i} + \sum_{r=1}^{3} c_r(e^{-\alpha_r \Delta z_i} - 1) \left.\frac{\partial \underset{\sim}{e}^p}{\partial z}\right|_{z=z_i} \quad (i = 1,..m \tag{4.5}$$

where $\underset{\sim}{h}(0) = 0$ and $\Delta z_i = z_i - z_{i-1}$.

This is an important result to the effect that the history dependence of the material response (through $\underset{\sim}{h}(z_i)$) at the intrinsic time z_i will be determined by $\underset{\sim}{h}(z_{i-1})$ and the new incremental step (through $\left.\frac{\partial \underset{\sim}{e}^p}{\partial z}\right|_{z=z_i}$ and z_i). This formula is also of value in the computer program, because (a) one need only store the information at z_{i-1} to obtain results at z_i, and (b) when using (4.5) instead of equation (4.4), the value of the term $\exp(\alpha_r \Delta z_i)$ is no longer small thus avoiding truncation errors present in the previous formulation (equation 4.4).

THE ITERATIVE PROCESS

For every increment of loading or unloading an initial value Δz^o is assigned to the increment of intrinsic time. The linear simultaneous equations are then solved and the displacement increments are obtained, from which the total deviatoric strain $\Delta \underset{\sim}{e}$ is calculated. Also $\Delta \underset{\sim}{s}$ and $\Delta \underset{\sim}{e}^p$ are calculated using equations (2.10) and (2.3) respectively. Upon use of equations (2.1a), (2.1b) and (4.5) Δz, $\frac{\partial \underset{\sim}{e}^p}{\partial z}$ and $\underset{\sim}{h}$ are obtained. Also, from equations (2.17)-(2.19) or (2.22)-

(2.24) ΔH_{px}, ΔH_{py}, ΔH_{pxy} and finally (ΔP_p) are obtained. Substituting $\{\Delta P_p\}$ into the simultaneous equations (4.2) we then obtain a new solution for the displacement increments as well as the other variables, including Δz. The iteration process is continued until the difference in two consecutive values of Δz, corresponding to two consecutive iterations, is less than some defined tolerance. Results are stored for the next step. The new loading process is then repeated.

In this initial stress method of classical plasticity one [12] usually stops the iteration process if the difference in the magnitudes of the plastic pseudo-force vector corresponding to two consecutive iterations is sufficiently small. We use the scale Δz as a criterion of convergence instead of the pseudo-force vector, not only because of its simplicity but because of its crucial role in endochronic plasticity.

CONVERGENCE AND TOLERANCE

The rate of convergence is very important because it relates to consumption of computer time, truncation error and other related considerations. The key of accelerating the convergence rate is how to choose the initial Δz in order to begin the iteration process of a new incremental loading (unloading) step. An accelerator K_a was used to determine the starting value of the increment of intrinsic time Δz_I^o by the relation

$$\Delta z_I^o = K_a^I \Delta z_{I-1}^L \qquad (6.1)$$

where the subscript I denotes the current incremental loading step and I-1 denotes the preceding step. The superscript o denotes the initial value, L denotes the last value and K_a^I is called the accelerator for the I'th increment. Equation (6.1) is not suitable for reversal points, at which Δz_I^o is taken equal to zero, because at the onset of unloading the response is elastic. The value of the accelerator was determined by the ratio of the final value of Δz in the two previous steps, i.e.,

$$K_a^I = \frac{\Delta z_{I-1}^L}{\Delta z_{I-2}^L} \tag{6.2}$$

With the exception of the first few (three) increments the value of K_a^I was substantially constant. To illustrate its utility and average value of 1.24 was used and the number of iterations needed for convergence was compared in cases where $K_a^I = 1$ and $K_a^I = 0$. See Fig. 2 where n pertains to the fifteenth increment and ε^{yp} is the plastic strain near the tip of the notch. Curve 1 ($K_a = 0$) shosws that the convergent process is very slow. The reason is that at the first iteration $\Delta z_I^o = 0$ since $K_a = 0$ and therefore $\{\Delta P\}^P = 0$, i.e., the loading process so initiated is elastic and is far away from the real case. Curve 2($K_a = 1$) shows the convergent rate is much better than in curve 1, because it takes the final value of Δz in the previous incremental loading step as the initial value of Δz in the current step. However, in this procedure the plastic pseudo-load is underestimated. A value of K_a greater than

unity does increase the rate of convergence as shown in curve 3 ($K_a = 1.24$). Figure 3 shows the effect of accelerator factor K_a on the average iteration number N_{ave} per incremental loading step.

By definition the relative error ERR is defined as

$$ERR = \frac{\Delta z_n - \Delta z_{n-1}}{\Delta z_n} \qquad (4.41)$$

where n is the number of iteration steps. Tolerance is defined as the maximum acceptable value of ERR. Figures 4 and 5 show the effect of tolerance on the accuracy and rate of convergence. In the example shown the smaller the tolerance the higher the accuracy (Fig. 4), but the number of iterations increases (Fig. 5). One however must guard against an excessively small tolerance, which may lie outside the inherent accuracy of the numerical computation and computer capability, leading to accumulation of truncation errors. In the present work the tolerance was 1%.

COMPARISON BETWEEN EXPERIMENTAL DATA AND CALCULATED RESULTS

To verify the validity of the endochronic analysis, using the present numerical algorithm, the distribution of strain of a notched specimen (made of OFHC copper) cyclicly loaded in its own plane was calculated and measured. One quarter of the specimen is shown in Fig. 6. The material functions $\rho(z)$ and $f(\zeta)$ were determined by means of an experiment on a round

specimen of precisely the same material as the notched specimen, in terms of purity, grain size and treatment. The method of determination of these functions will not be given here but may be found in Ref. 13. Suffice it to say that they are of the following form:

$$\rho(z) = \sum_{r=1}^{3} A_r e^{-\alpha_r z} \qquad \text{(GPA)}$$

where $A_{1,2,3} = (592, 220, 46)$ and $\alpha_{1,2,3} = (27.5, 11.5, 7.67) \times 10^3$ and

$$f(\zeta) = 1 + 0.53\zeta^{0.72}$$

The calculations were conducted on an electronic computer (AMDAHL 470 V/7A, close to IBM 370) in the computer center of the University of Cincinnati. There are 413 elements and 230 nodes in one quarter of the specimen (Fig. 6). The side of the smallest element is 0.25 mm. By "varying band storage" the amount of storage for the total stiffness matrix is 17698. The incremental loading for each step is 4% of the maximum load. The average number of iterations for each incremental loading was about 10, varying from 3 to 20. The computer time for each iteration was about 3.36 sec., most of which is used to solve the 460 simultaneous equations. The experiments were conducted in Metcut Research Associates Corporation. The strain distribution was measured using strain gauges, the smallest nominal length of which was 0.2 mm. Since the locations of the elements and the strain gauges did not coincide exactly, we compared the calculated results with experimental data in terms of plotted curves. Comparisons were made over a wide

range of magnitude of applied maximum stress, location and type of histories.

Measured and Calculated Strain Distributions ε_y Along the Notch Center Line oo' are Shown, for Applied Stress Amplitude 3.7×10^7 PA

(i) at first tensile peak A. Fig. 7

(ii) at first unloading point C. Fig. 8

(iii) at first compressive loading peak B. Fig. 9

Letter designations as shown in those Figures.

Measured and Calculated Strain Distributions ε_y Along the Vertical Line ob are Shown for Applied Stress Amplitude 2.3×10^7 PA

(i) at first tensile peak E. Fig. 10

(ii) at first compressive peak L. Fig. 11

(iii) at second loading peak H. Fig. 12

Letter designations as shown in above figures.

Despite the complexity of the boundary value problem and the inherent experimental difficulties the agreement between experimental and calculated results is excellent both from the aspect of tendency and magnitude.

REFERENCES

1. Lamba, H.S. and Sidebottom, O.M., "Biaxial Cyclic Hardening of Anealed Copper Cylinders Evaluated by Deformation Plasticity Theories," T. & A.M. Report No. 406 (1976), The University of Illinois, Urbana-Champaign.

2. Hunsaker, B. Jr., Vanghan, D.K. and Stricklin, J.A., "A Comparison of the Capacity of Four Hardening Rules to Predict a Material's Plastic Behavior," TEES-RPT-2926-73-3, Oct. 1973. Aerospace Engineering Department, Texas A. & M. University, College Station, Texas.

3. Tanaka, M., "Large Deflection Analysis of Elastic-Plastic Circular Plates with Combined Isotropic and Kinematic Hardening," Ingenicur-Archiv 41, 1972, pp. 342-356.

4. Haythronthwaite, R.M., "A More Rational Approach to Strain Hardening Data," Engnr. Plasticity, J. Heymon & F.A. Leckie, (ed.), Cambridge Press, 201 (1968).

5. Valanis, K.C., "A Theory of Viscoplasticity Without a Yield Surface, Part I. General Theory," Archives of Mechanics, 1971, pp. 517-533.

6. Valanis, K.C., "A Theory of Viscoplasticity without a Yield Surface. Part II. Application to Mechanical Behavior of Metals," Archives of Mechanics, 1971, pp. 535-551.

7. Valanis, K.C., "Endochronic Theory with Proper Hysteresis Loop Closure Properties," Systems, Science and Software Report SSS-R-80-4182, 1979.

8. Valanis, K.C. and Read, H., "New Endochronic Plasticity Model for Soils," Soil Mechanics - Transient and Cyclic Loads. Ed. G.N. Pande and O.C. Zienkiewicz, John Wiley and Sons, 1982.

9. Valanis, K.C. and Lee, C.F., "Some Recent Developments of the Endochronic Theory with Applications," Nuclear Eng. and Design, 69, 1983, pp. 327-343.

10. Lin, H.C. and Wu, H.C., "On the Improved Endochronic Theory of Viscoplasticity and It's Application to Plastic-Wave Propagation," to be published in Int. J. Solids Structures.

11. Argyris, J.H., "Energy Theorems and Structural Analysis," Butterworth, 1960. (Reprinted from Aircraft Eng., 1954-1955).

12. Zienkiewicz, O.C., Valliappan, S. and King, I.P., "Elasto-plastic Solutions of Engineering Problems 'Initial Stress', Finite Element Approach," International Journal for Numerical Methods in Engineering. Vol. 1, 1969, pp. 75-100.

13. Fan, Jinghong, "A Comprehensive Numerical Study and Experimental Verification of Endochronic Plasticity," Ph.D. Dissertation, Department of Aerospace Engineering and Applied Mechanics, University of Cincinnati, 1983.

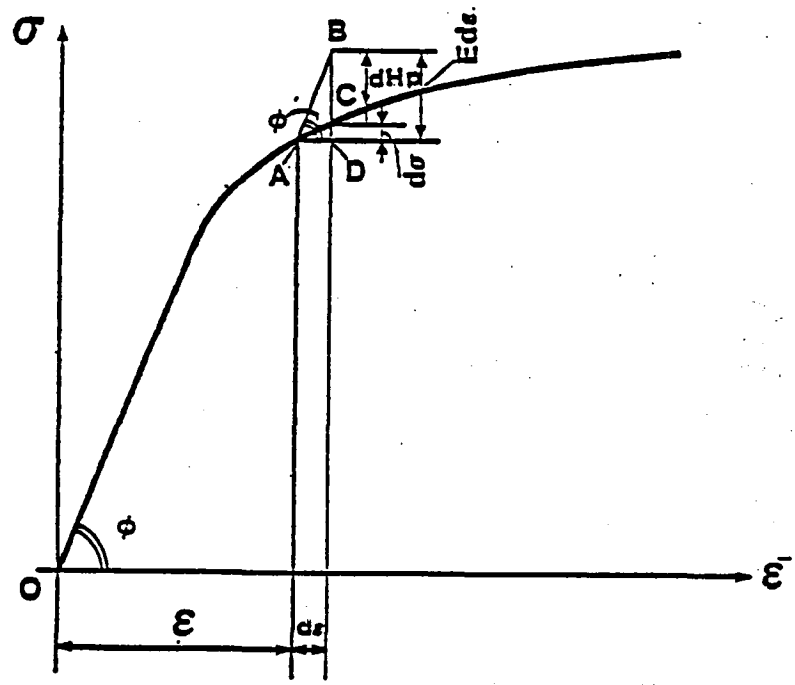

Figure 1. - The Geometric Meaning of The Incremental Endochronic Elastoplastic Constitutive Equation

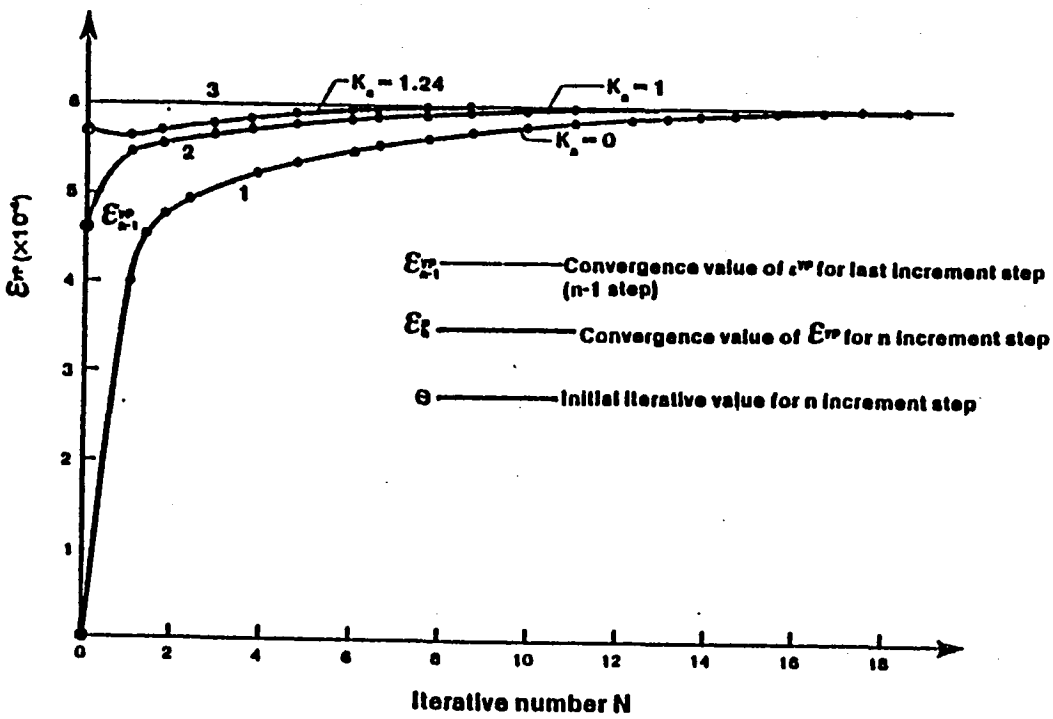

Figure 2. - The Effect of Acceleration Factor K_a on the Convergence of ε^{vp}_{max}

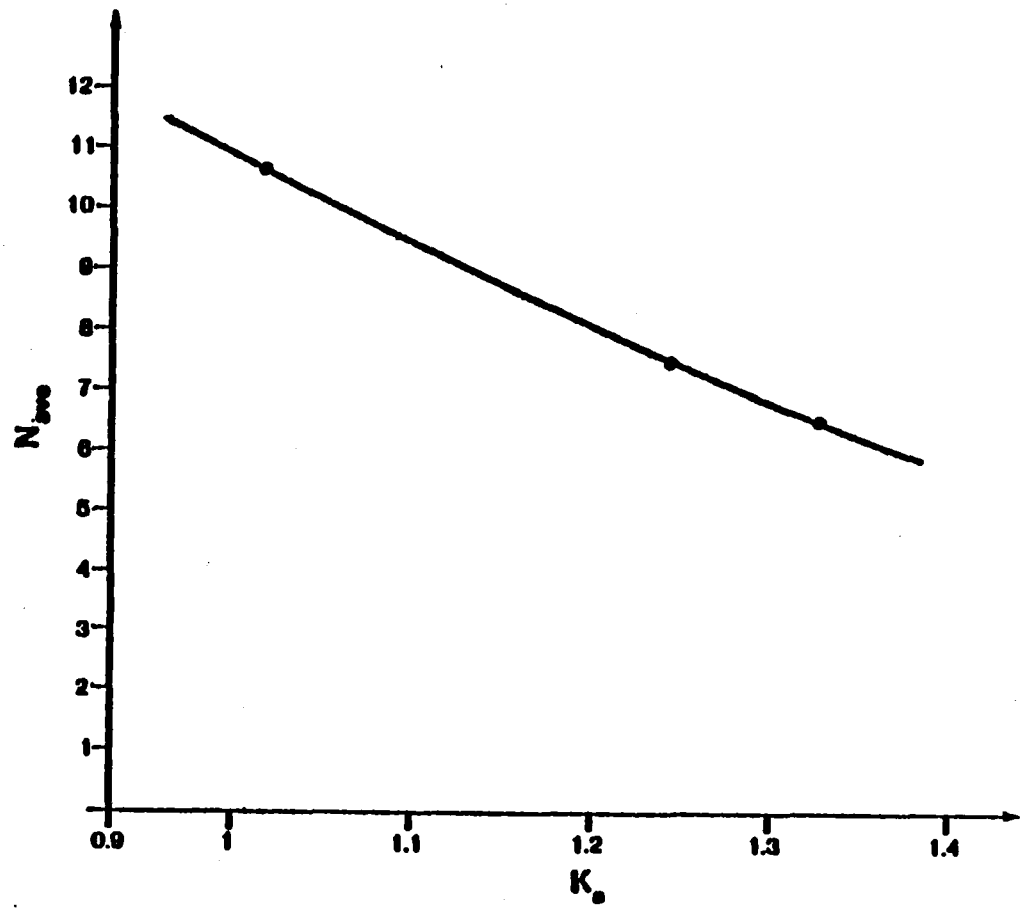

Figure 3. - The Effect of Acceleration Factor K_a on the Average Iteration Numbers per Incremental Loading Step

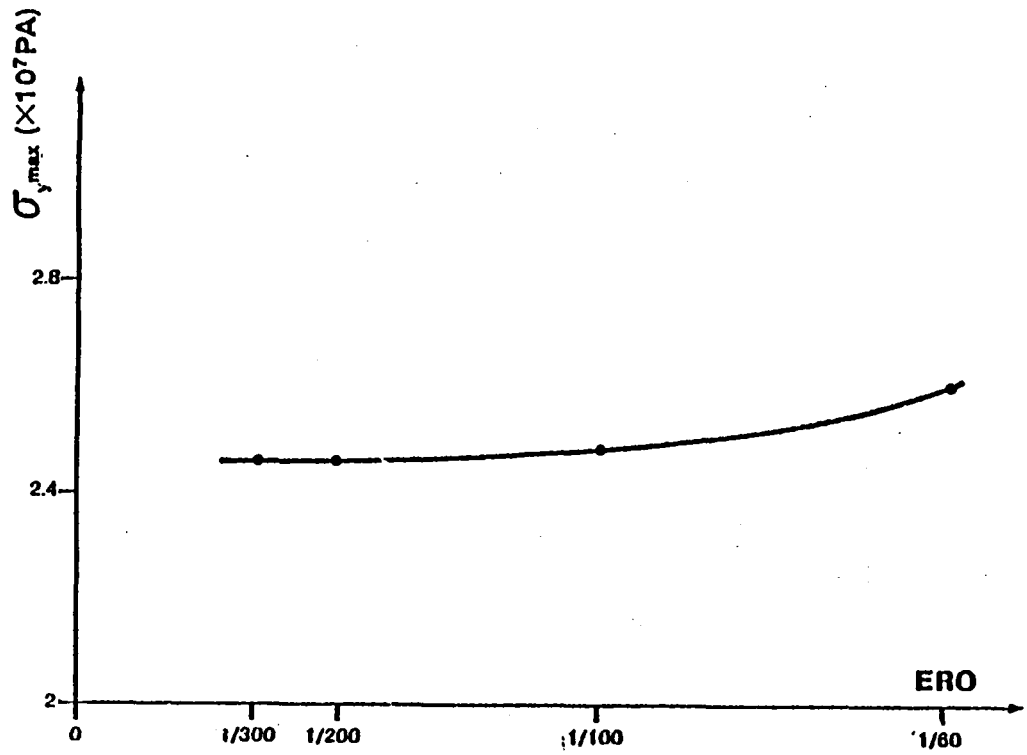

Figure 4. - The Effect of Tolerance on the Magnitude of $\sigma_{y_{max}}$

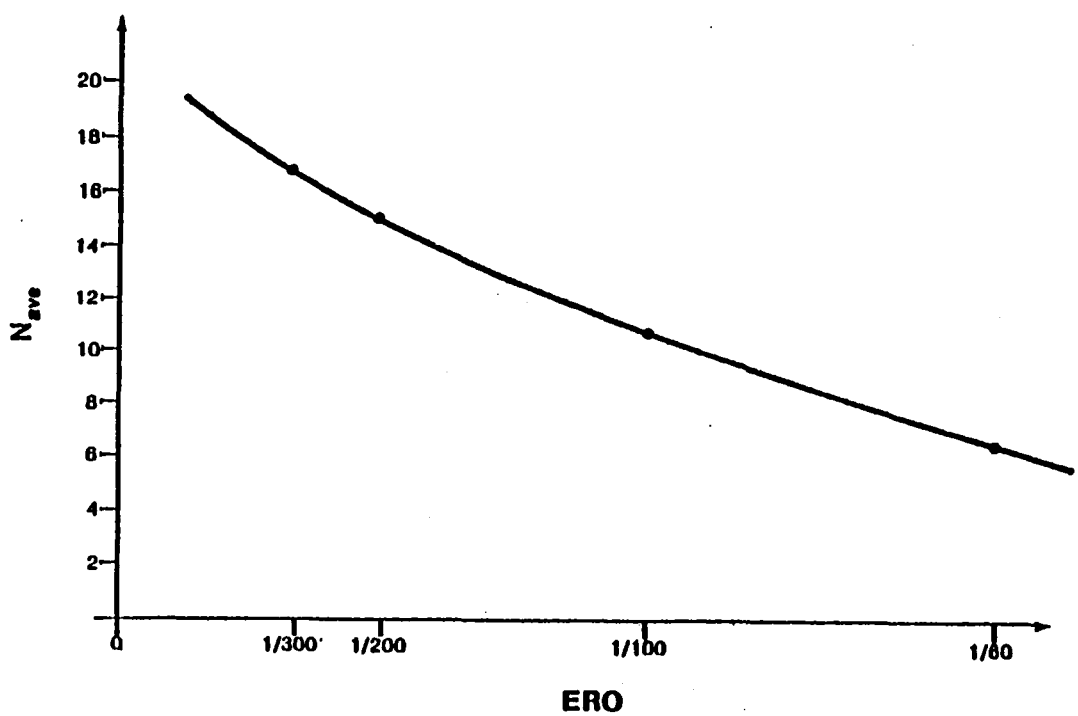

Figure 5. - The Effect of the Tolerance on the Average Iteration Number per Incremental Loading Step

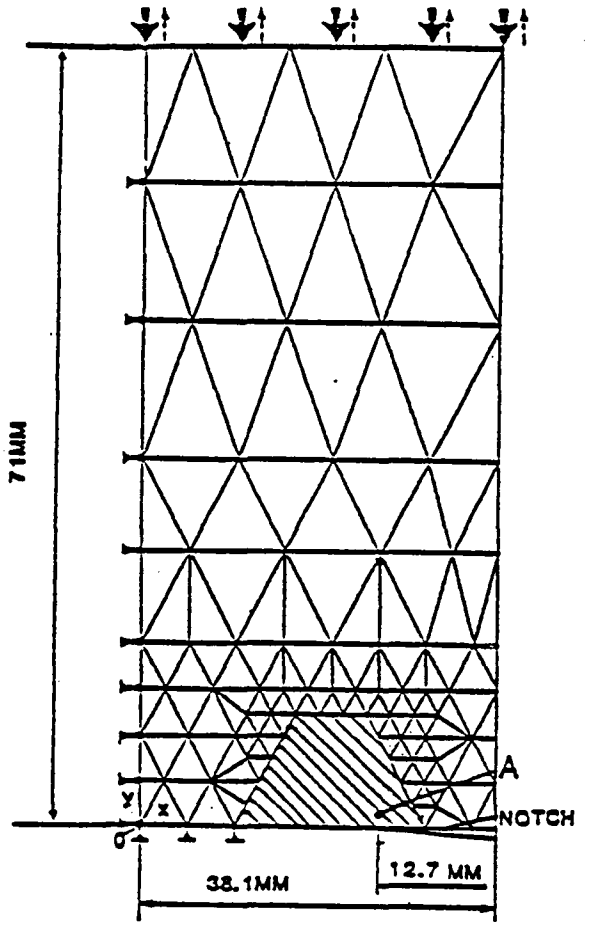

(a) Coarse Mesh

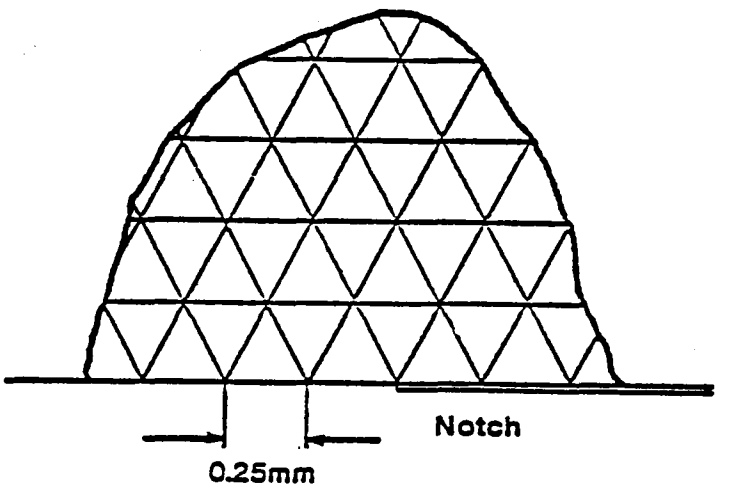

(b) Fine Mesh Near the Notch Tip

Figure 6. - Plate Geometry and Grid Arrangement (one quarter)

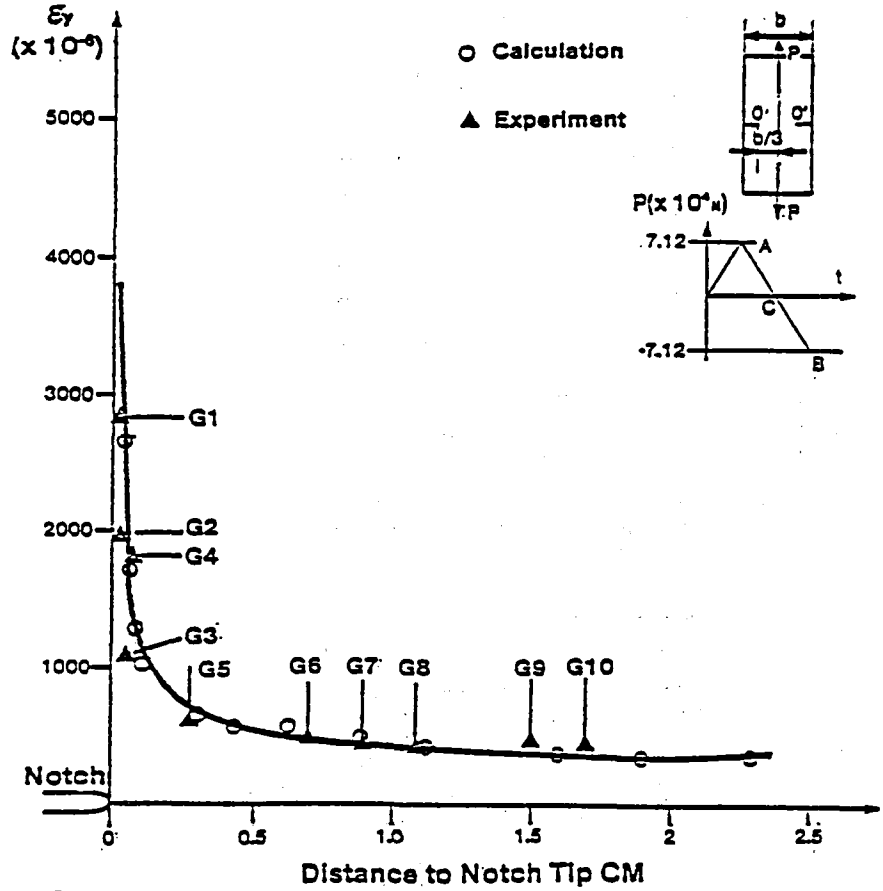

Figure 7. – Comparison Between Experimental and Calculated Distribution of Strain ε_y Along Notch Line OO' at Positive Peak A

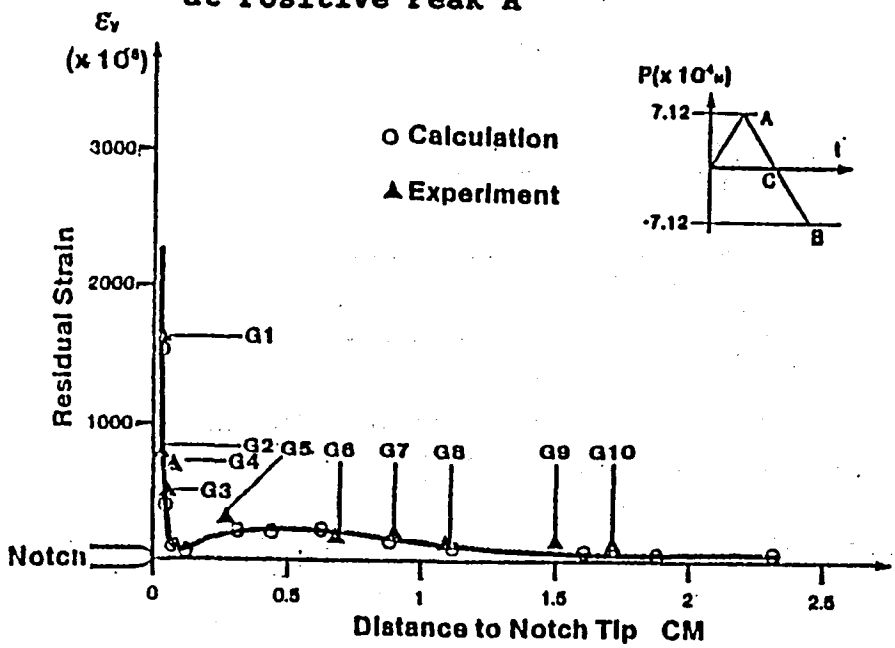

Figure 8. – Comparison Between Experimental and Calculated Residual Strain Distribution ε_y Along Notch Line OO' at Point C

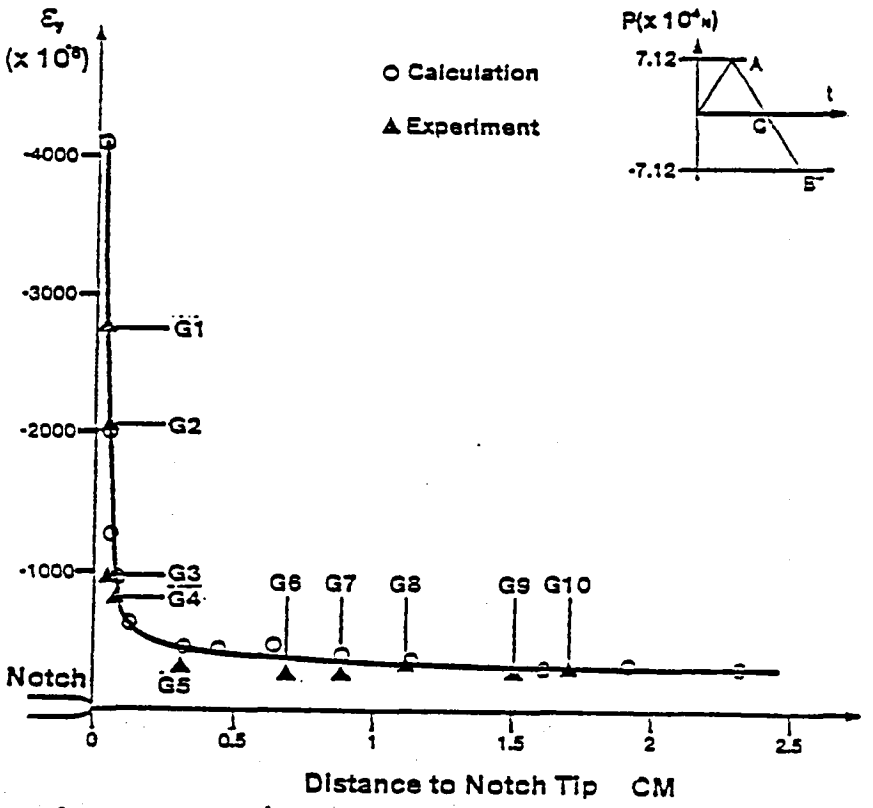

Figure 9. - Comparison Between Experimental and Calculated Strain Distribution ε_y Along Notch Line OO' at Negative Peak B

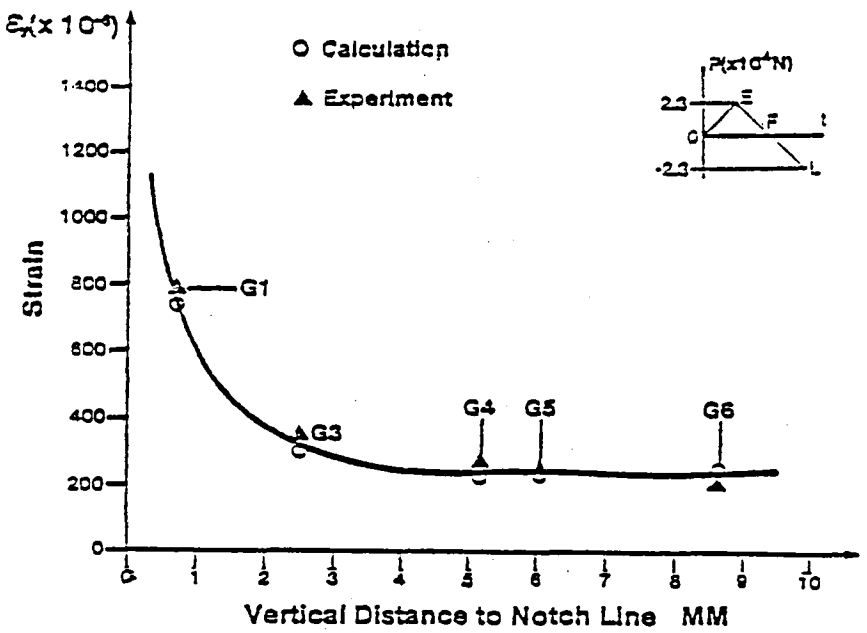

Figure 10. - Comparison Between Experimental and Calculated Strain Distribution ε_y at the Positive Peak E Along the Vertical Line ob at the Top of Notch Tip

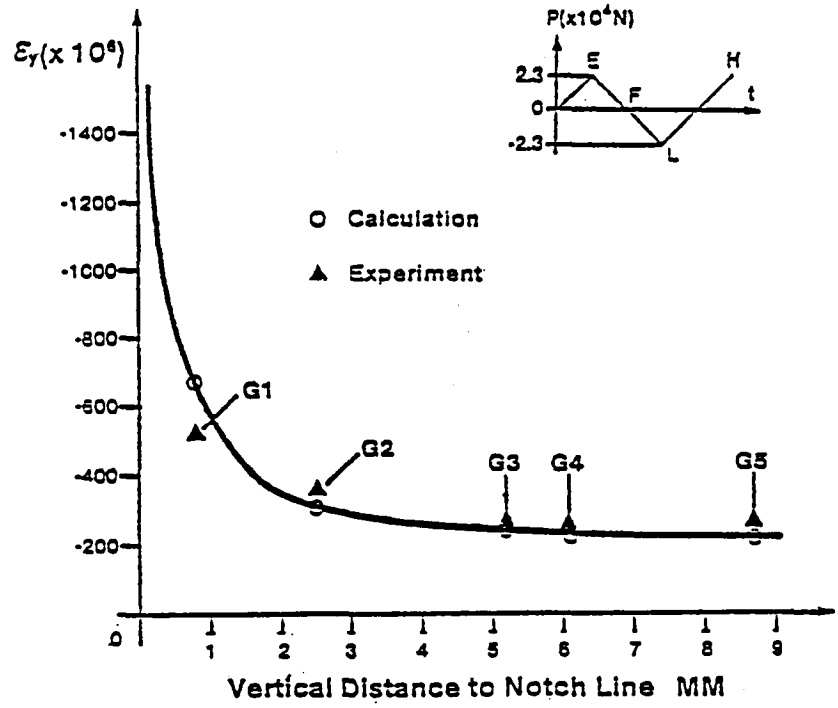

Figure 11. - Comparison Between Experimental and Calculated Strain Distribution ε_y at the Negative Peak L Along the Vertical Line ob at the Top of Notch Tip

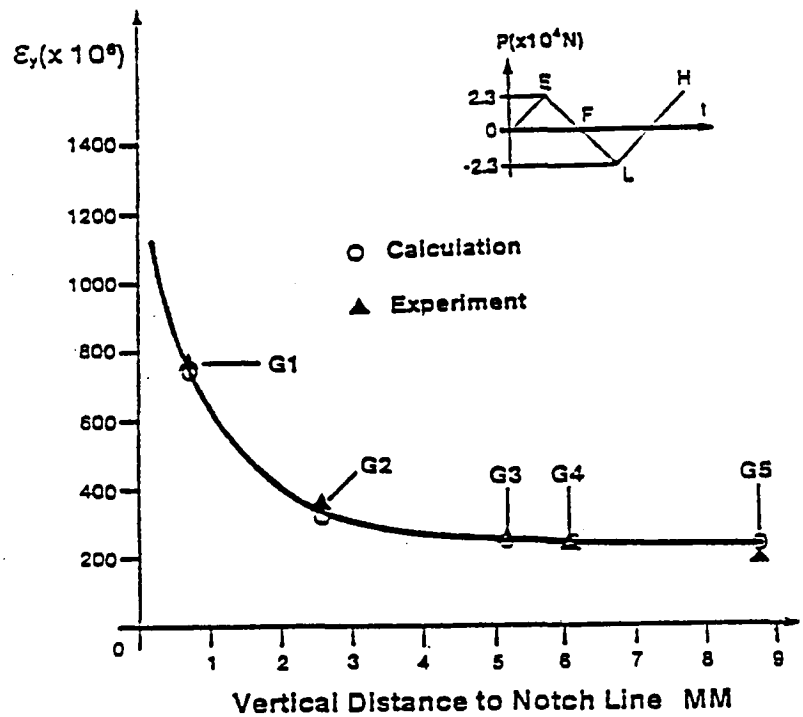

Figure 12. - Comparison Between Experimental and Calculated Strain Distribution ε_y at the Positive Peak E Along the Vertical Line ob at the Top Notch Tip